

T_{eff} and $\log g$ dependence of velocity fields in M-stars

S. Wende*, A. Reiners* and H.-G. Ludwig†

**Institut für Astrophysik, Georg-August-Universität Göttingen, Friedrich-Hund Platz 1, D-37077 Göttingen, Germany*

†*GEPI, CIFIST, Observatoire de Paris-Meudon, 5 place Jules Janssen, 92195 Meudon Cedex, France*

Abstract. We present an investigation of velocity fields in early to late M-type hydrodynamic stellar atmosphere models. These velocities will be expressed in classical terms of micro- and macro-turbulent velocities for usage in 1D spectral synthesis. The M-star model parameters range between $\log g$ of 3.0 – 5.0 and T_{eff} of 2500 K – 4000 K. We characterize the T_{eff} - and $\log g$ -dependence of the hydrodynamical velocity fields in these models with a *binning* method, and for the determination of micro-turbulent velocities, the *Curve of Growth* method is used. The macro-turbulent velocities are obtained by convolutions with Gaussian profiles. Velocity fields in M-stars strongly depend on $\log g$ and T_{eff} . Their velocity amplitudes increase with decreasing $\log g$ and increasing T_{eff} . The 3D hydrodynamical and 1D macro-turbulent velocities range from ~ 100 m/s for cool high gravity models to ~ 800 m/s–1000 m/s for hot models or models with low $\log g$. The micro-turbulent velocities range in the order of ~ 100 m/s for cool models, to ~ 600 m/s for hot or low $\log g$ models. Our M-star structure models are calculated with the 3D radiative-hydrodynamics (RHD) code CO⁵BOLD. The spectral synthesis on these models is performed with the line synthesis code LINFOR3D.

Keywords: Radiative transfer - Line: profiles - Stars: atmospheres, low-mass, kinematics

PACS: 95.30.Jx, 95.30.Ky, 95.30.Lz, 95.75.Fg

INTRODUCTION

The measurement of line broadening in cool stars is in general a difficult task. For example, the investigation of the rotation-activity connection among field M-dwarfs requires the measurement of rotational line broadening with an accuracy of 1 km/s [1]. The spectral lines have to be very narrow and well isolated to detect slow rotation. But in cool stars most of the individual atomic lines become very weak at these low temperatures and are dominated by pressure broadening. Also the measurement of the magnetic field strength is dependent on the line width, and detection of Zeeman splitting becomes more difficult at low temperatures due to the aforementioned reasons. Since it is possible to use the narrow and well isolated FeH molecule lines in cool stars to determine radial velocities or magnetic field strength [2], it would be very helpful to characterize the impact of macroscopic velocity fields – primarily driven by convection – on the line shapes from hydrodynamical model atmospheres. We calculate 3D-CO⁵BOLD stellar atmosphere models [3] which serve as input to the line formation program LINFOR3D [based on 4]. Velocity fields and thermal inhomogeneity are naturally represented in the hydrodynamical models. The influence on the modeled spectral lines can then be investigated and translated into effective micro- and macro-turbulent velocities used

in classical analyses based on 1D hydrostatic model atmospheres. The comparison with 1D-models provides some insight when it is necessary to apply 3D-models in the spectral analysis of cool stars.

In the first part of the paper we describe our hydrodynamical model atmosphere code and give an overview of the models, in the second part we investigate the velocity fields in the models and their dependence on $\log g$ and T_{eff} . We will express the influence of velocity fields on line shapes in terms of micro- and macro-turbulent velocities.

METHODS AND MODELS

CO⁵BOLD is the abbreviation for ‘‘COnservative COde for the COmputation of COmpressible COnvection in a BOx of L Dimensions with L=2,3’’ [5]. It can be used to model solar and stellar surface convection. In solar-like stars, a CO⁵BOLD model represents the 3D flow geometry and its temporal evolution in a small (relative to the star’s radius) Cartesian domain at the stellar surface (‘‘box in a star’’ set-up). The spatial size of the domain is chosen to be sufficient to include the dominant convective scales, i.e. the computational box is large enough to include a number of granular cells at any instant in time. A CO⁵BOLD model provides a statistical realization of the convective flow. In this investigation we usually average over five flow fields taken at different instances in time (‘‘snapshots’’) to improve the statistics.

CO⁵BOLD solves the coupled non-linear time-dependent equations of compressible hydrodynamics coupled to the radiative transfer equation in an external gravitational field in 3 spatial dimensions. As set of independent quantities are chosen the mass density ρ , the three spatial velocities v_x , v_y , and v_z , and the internal energy ε_i . With these quantities, the 3D hydrodynamics equations, including source terms due to gravity, are the mass conservation equation

$$\frac{\partial \rho}{\partial t} + \frac{\partial \rho v_x}{\partial \rho x} + \frac{\partial \rho v_y}{\partial \rho y} + \frac{\partial \rho v_z}{\partial \rho z} = 0, \quad (1)$$

the momentum equation

$$\frac{\partial}{\partial t} \begin{pmatrix} \rho v_x \\ \rho v_y \\ \rho v_z \end{pmatrix} + \frac{\partial}{\partial x} \begin{pmatrix} \rho v_x v_x + P \\ \rho v_y v_x \\ \rho v_z v_x \end{pmatrix} + \frac{\partial}{\partial y} \begin{pmatrix} \rho v_x v_y \\ \rho v_y v_y + P \\ \rho v_z v_y \end{pmatrix} + \frac{\partial}{\partial z} \begin{pmatrix} \rho v_x v_z \\ \rho v_y v_z \\ \rho v_z v_z + P \end{pmatrix} = \begin{pmatrix} \rho g_x \\ \rho g_y \\ \rho g_z \end{pmatrix}, \quad (2)$$

and the energy equation which includes the radiative heating term Q_{rad}

$$\frac{\partial \rho \varepsilon_{ik}}{\partial t} + \frac{\partial (\rho \varepsilon_{ik} + P) v_x}{\partial x} + \frac{\partial (\rho \varepsilon_{ik} + P) v_y}{\partial y} + \frac{\partial (\rho \varepsilon_{ik} + P) v_z}{\partial z} = \rho (g_x v_x + g_y v_y + g_z v_z) + Q_{\text{rad}}. \quad (3)$$

ε_{ik} denotes the sum of internal and kinetic energy. The gas pressure P is related to density ρ and internal energy ε_i via a (tabulated) equation of state $P = P(\rho, \varepsilon_i)$. For the

local models used here the gravity field is given by the constant vector $\vec{g} = \begin{pmatrix} 0 \\ 0 \\ -g \end{pmatrix}$.

CO⁵BOLD uses the convention that the vertical axis points upwards. The radiative heating term Q_{rad} is obtained from the solution of the non-local frequency-dependent radiative transfer equation. The frequency dependence of the radiation field is captured by considering a small number of representative wavelength bands [“opacity binning”, see 3, 6]. The resulting 3D radiative-hydrodynamic (RHD) models treat convection from basic physical principles and avoid approximations like mixing-length theory. In the following, the three dimensional data cubes of the CO⁵BOLD-models will be called “3D-models”, and the spectral lines computed from three dimensional atmosphere models “3D-lines”.

We will characterize the velocity fields in the 3D RHD models and analyze their influence of FeH lines. For the 1D spectral synthesis the 3D velocity fields will be expressed in terms of micro- and macro-turbulent velocity. For this investigation, we choose a set of CO⁵BOLD-models with $T_{eff} = 2500 \text{ K} - 4000 \text{ K}$ and $\log g = 3.0 - 5.0$ [cgs]. Table 1 gives the model parameters. The opacities used in all models are obtained

TABLE 1. Overview of different model quantities. We simulated main sequence stars and varied $\log g$ slightly for models with changing T_{eff} . The models with almost same T_{eff} were started at the same T_{eff} of 3300 K, but they converge at slightly lower or higher T_{eff} .

Model code	Dim.	Size(x,y,z) [km]	Opacities	T_{eff} [K]	$\log g$ [cgs]
d3t33g30mm00w1	3	85000 x 85000 x 58350	PHOENIX	3240	3.0
d3t33g35mm00w1	3	28000 x 28000 x 11500	PHOENIX	3270	3.5
d3t33g40mm00w1	3	7750 x 7750 x 1850	PHOENIX	3315	4.0
d3t33g50mm00w1	3	600 x 600 x 260	PHOENIX	3275	5.0
d3t40g45mm00n01	3	4700 x 4700 x 1150	PHOENIX	4000	4.5
d3t38g49mm00w1	3	1900 x 1900 x 420	PHOENIX	3820	4.9
d3t35g50mm00w1	3	1070 x 1070 x 290	PHOENIX	3380	5.0
d3t28g50mm00w1	3	370 x 370 x 270	PHOENIX	2800	5.0
d3t25g50mm00w1	3	240 x 240 x 170	PHOENIX	2575	5.0

from the PHOENIX stellar atmosphere package [7] assuming an abundance mixture according Asplund et al. [8]. The opacity tables were computed after Ferguson et al. [9] and Freytag et al. [10].

In order to compare 1D model atmospheres with the hydrodynamical 3D-models, we average the 3D-models over surfaces of equal optical depth. We obtain so-called <3D>-models which have the same mean thermal profile as in the 3D-models but without cold and hot regions which stem from the convective granulation pattern. In the <3D>-models the hydrodynamic velocity field is not considered. The line-broadening is treated in the classical way by adding isotropic Gaussian micro- and macro-turbulence. We will call the spectral lines of these models <3D>-lines.

HYDRODYNAMICAL VELOCITY FIELDS

Spectral lines are broadened by velocity fields where the wavelength of absorption or emission of a particle is shifted due to its motion in the gas. Here we are mostly concerned with the macroscopic, hydrodynamic motions but have in mind that the thermal motions are also constituting an important contribution. If we envision each voxel in the RHD model cube to form its own spectral line, the whole line consists of

a (weighted) sum of single lines. The velocity distribution might be represented by a histogram of the velocities of the voxels. We try to describe the velocity fields in that sense instead of using the rms-velocities. Since a velocity vector is assigned to each voxel, we apply a binning method and count all vertical velocities to plot them in a histogram with a bin size of 25 m/s. We took the standard deviation σ of a fitted Gaussian normal distribution as a measure for the velocity dispersion in the models (see Fig.1). At this stage of the investigation time we only concentrate on the vertical direction which is appropriate if we assume that the major part of the line broadening stems from the vertical motions. The velocities of the horizontal directions are of roughly the same order. As a measure for the statistical variability in the 3D RHD model, we average

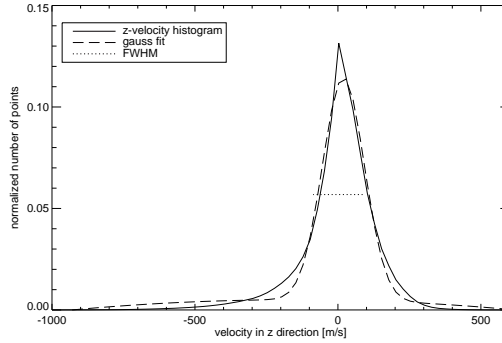


FIGURE 1. Histogram of the velocity distribution in vertical direction. The normalized number of points is plotted against the vertical velocity in m/s (solid line). The Gaussian (dashed line) fits the velocity distribution and determined an FWHM value (dashed-dotted line), which is related to σ with $FWHM = 2\sqrt{2\ln 2} \cdot \sigma$. The underlying model is located at $T_{\text{eff}} = 2800$ K and $\log g = 5$ [cgs].

over five different temporal windows and also compute the standard deviation. The determined velocities are plotted against T_{eff} and $\log g$ to investigate their dependence (Fig. 2). The velocities increase strongly with decreasing $\log g$ and with increasing T_{eff} . They are as low as a few hundred m/s in the coolest high-gravity models. We can describe the dependence of the velocity dispersions on T_{eff} with a second order polynomial, and in $\log g$ with a linear function (The fits for the velocity dispersion are overplotted in Fig.2).

In order to investigate in which region of the model atmospheres the velocity fields are generated and what the physical meaning of the σ is, we bin the 3D model velocities at constant geometrical height and fit a Gaussian to determine the velocity dispersion for each layer (Fig. 3). Typically, we find maxima of the velocity dispersion around $\log \tau = -1$. The maximum velocities in the convection zone of each model (T_{eff} and $\log g$) are plotted in Fig. 2 too. In order to measure the velocities in the region where the lines originate, we compute the mean of the velocities weighted with the contribution function of the line depression [11] $\sigma_{\text{weighted}} = \frac{\sum_{\tau=2}^{-6} \sigma_{\tau} \cdot CF_{\tau}}{\sum_{\tau=2}^{-6} CF_{\tau}}$ showed in the bottom panel of Fig. 3. These velocities are also plotted in Fig. 2. In most cases they lie between the velocity dispersion and the maximum velocity in the convection zone. Some models show a strong increase of the vertical velocity in higher layers (Fig. 3). This is related to the presence of waves which are excited by the stochastic fluid motions [3, and references therein]. However, it will not affect the spectral lines, because they are

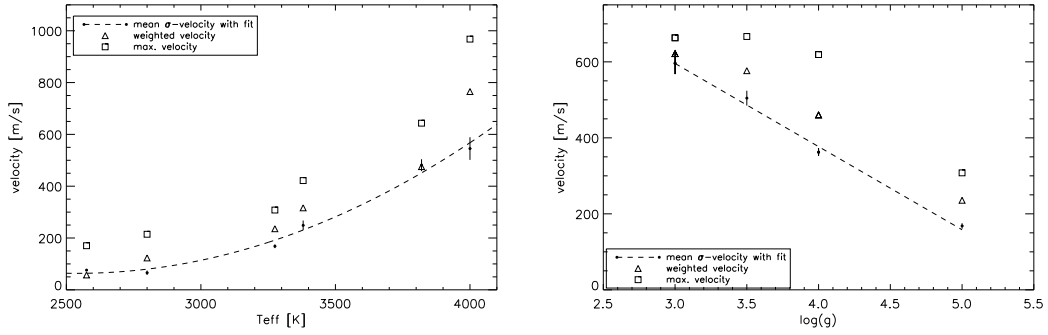


FIGURE 2. Plotted are velocity dispersions with error bars, maximal velocities in the convection zone, and weighted velocity dispersions (see text) for models with different T_{eff} (left) and different $\log g$ (right). The dashed line on the left plot shows a second order polynomial fit for the velocity dispersion and on the right plot a linear function is sufficient to fit the $\log g$ data.

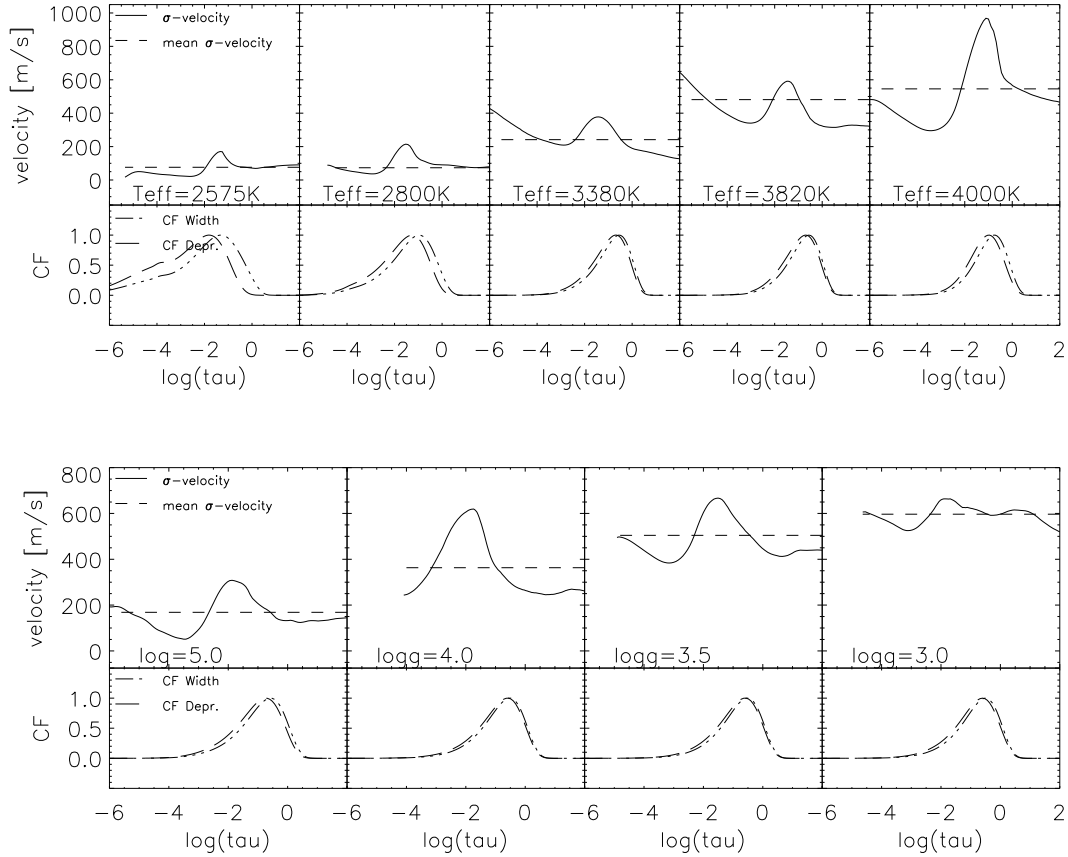


FIGURE 3. Upper panel: σ velocities. In each upper panel the σ -velocities (solid) and the mean σ -velocity (dotted) are plotted against the optical depth in logarithmic scale. Bottom panel: In each bottom panel are the contribution functions (CF) of a FeH-line at a wavelength of 9954.0 Å. The width (dashed) and depression (dotted) of the line as a function of optical depth on a logarithmic scale.

generated in the region between an optical depth of $\log \tau = 1.0$ and $\log \tau = -4.0$.

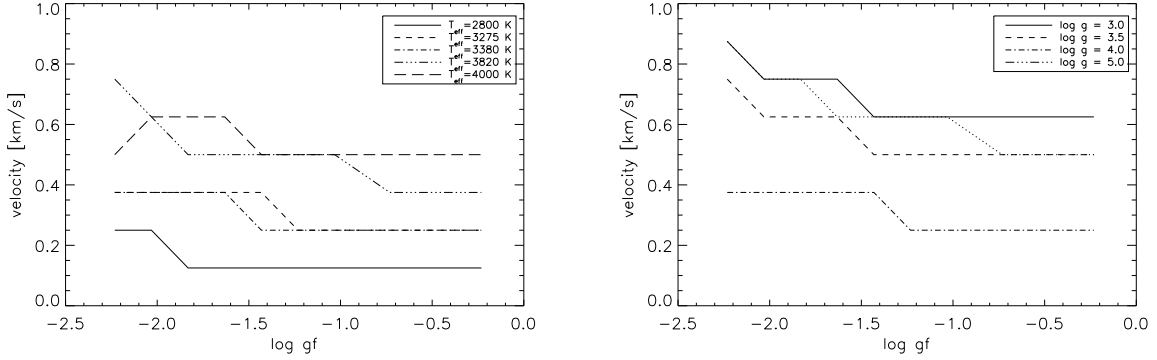


FIGURE 4. Micro-turbulent velocities as a function of $\log gf$ for different T_{eff} (left) and different $\log g$ (right).

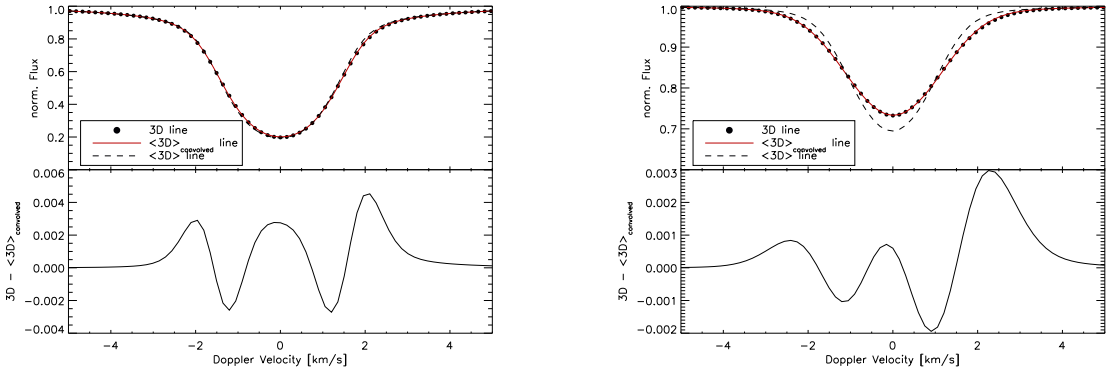


FIGURE 5. FeH lines for models with $T_{\text{eff}} = 2800$ K, $\log g = 5.0$ [cgs] (left) and $T_{\text{eff}} = 3820$ K, $\log g = 4.9$ [cgs] (right). The upper panels show the 3D-line (dots) and the $\langle 3D \rangle_{\text{convolved}}$ -line (solid line) which was broadened by a Gaussian profile. For comparison we plotted a $\langle 3D \rangle$ -line which was not broadened by any velocities (dashed line). In the lower panels are the $3D - \langle 3D \rangle_{\text{convolved}}$ residuals plotted. One can see the asymmetry which stems from the line shifts due to convective motions.

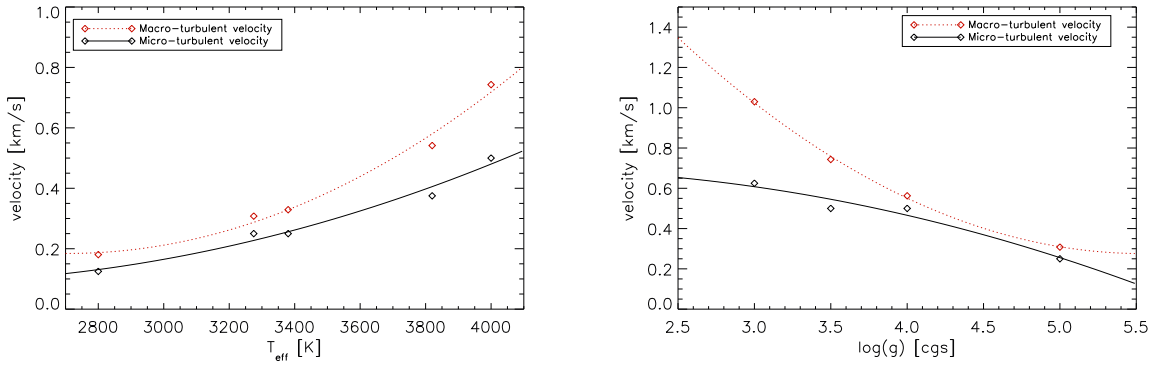


FIGURE 6. Micro- and macro-turbulent velocities as a function of T_{eff} (left) and $\log g$ (right). The data points are fitted by second order polynomials.

MICRO- AND MACRO-TURBULENT VELOCITIES

In the following we express the 3D hydrodynamical velocities in terms of classical micro- and macro-turbulent velocities [see e.g. 12, 13]. We try to see how accurately the 1D broadening resembles the 3D broadening in the regime of cool stars which, as we saw, exhibit velocity fields of relatively small amplitudes. A 1D treatment would save a lot of CPU-time, and little differences between 1D and 3D broadening could favor the usage of fast 1D atmosphere codes to simulate M-stars for comparisons with observations, e.g. to determine rotational- or Zeeman-broadening.

Micro-turbulent velocities: In order to determine the micro-turbulent velocities, we use the *curve of growth* (CoG) method [13]. We increase the line strength of an FeH and an FeI line by (artificially) increasing the $\log gf$ value of the line which results in an increasingly saturated lines. In saturated lines, the effective absorbing cross-section is enhanced due to the influence of the micro-turbulent velocities. From 3D spectral synthesis we obtain a 3D CoG, which can we compare with the $\langle 3D \rangle$ CoG for different micro-turbulent velocities which are included in the 1D spectral synthesis. We use a grid of micro-turbulent velocities that range from 0 km/s to 1 km/s in 0.125 km/s steps and obtain $\langle 3D \rangle$ CoGs for nine different micro-turbulent velocities. We compare the $\langle 3D \rangle$ CoGs with the 3D CoG and select the velocity of the $\langle 3D \rangle$ CoG that fits the 3D CoG best. The determined velocities are plotted in Fig.6. Since strong (saturated) lines tend to be formed in the upper atmosphere, and weak (unsaturated) lines in deeper layers of the atmosphere, $\log gf$ and the height of formation are related. If we fit a micro-turbulent velocity to each $\log gf$ point of the 3D CoG, we obtain a height-dependent velocity structure (see Fig.4).

Macro-turbulent velocities: For modeling macro-turbulent broadening we used the radial-tangential profile from Gray [14], as well as a Gaussian profile in the 1D spectral synthesis. We compared $\langle 3D \rangle$ absorption lines which were broadened with both profiles, and the results differ only very little. Hence it is appropriate to use the Gaussian profile here. It is remarkable that the broadening due to small 3D RHD velocity fields in M-stars can be approximated with a simple Gaussian velocity distribution. Two examples of Gaussian broadened $\langle 3D \rangle$ FeH lines are shown in Fig. 5. To determine the macro-turbulent velocities of the 3D RHD models, we first compute the $\langle 3D \rangle$ lines with a given micro-turbulent velocity and after this we broaden them with a Gaussian with a given macro-turbulent velocity until they match the 3D profiles. The results are plotted in Fig.6. The broadened $\langle 3D \rangle$ FeH lines fit the 3D FeH lines very well. The difference of the $\langle 3D \rangle$ and 3D centroid ($C = \frac{\sum F \cdot v}{\sum F}$) range in the order of a few m/s for small velocity fields to 30 – 40 m/s for strong velocity fields in hot M star models, or models with low $\log g$. The differences stem from the asymmetry of the 3D line profiles, which are shifted due to convective motions. However, the errors in the normalized flux profiles are lower than 1% (see Fig. 5). We fit the micro- and macro-turbulent velocities as a function of T_{eff} and $\log g$, each pair can be fitted with a polynomial second order. The fits are overplotted in Fig.6. Both micro- and macro-turbulent velocities show similar dependence on T_{eff} and $\log g$ as the RHD velocity fields considered before (i.e. they increase with increasing T_{eff} and decreasing $\log g$). Especially the macro-turbulent velocities for changing T_{eff} agree well with the determined RHD velocities.

SUMMARY

We investigated the velocity fields in a set of M-star 3D hydrodynamical models. They range in T_{eff} and $\log g$ from $T_{\text{eff}} = 2500 \text{ K} - 4000 \text{ K}$ and $\log g = 3.0 - 5.0$ [cgs]. We applied a binning method to characterize the velocity structure and to determine mean velocities. These velocities range from $\sim 100 \text{ m/s}$ for the cool models up to $\sim 800 - 1000 \text{ m/s}$ for hot models or models with small $\log g$ values.

In order to compare the 3D RHD velocity fields with velocities needed in 1D spectral synthesis, we expressed them in terms of classical micro- and macro-turbulent velocities. For this purpose we computed the 3D and $\langle 3D \rangle$ *Curve of Growth* and determined the micro-turbulent velocity from them. They range in the order of $\sim 100 \text{ m/s}$ for cool models to $\sim 600 \text{ m/s}$ for hot models or models with small $\log g$. The macro-turbulent velocities were determined through convolution with a Gaussian profile which, what turns out, is sufficient in the regime of cool stars. The obtained velocities are of the order of the 3D RHD velocity fields and show similar dependence from T_{eff} and $\log g$. We saw that 1D spectral synthesis in cool stars with micro- and macro-turbulent velocity broadening is able to reproduce the 3D spectral line synthesis.

ACKNOWLEDGMENTS

SW would like to acknowledge the support from the DFG Research Training Group GrK - 1351 “Extrasolar Planets and their host stars”. AR acknowledges research funding from the DFG under an Emmy Noether Fellowship (RE 1664/4- 1). HGL acknowledges financial support from EU contract MEXT-CT-2004-014265 (CIFIST). We thank Derek Homeier for providing us with the opacity tables.

REFERENCES

1. A. Reiners, *A&A* **467**, 259–268 (2007).
2. A. Reiners, and G. Basri, *ApJ* **656**, 1121–1135 (2007).
3. H.-G. Ludwig, F. Allard, and P. H. Hauschildt, *A&A* **395**, 99–115 (2002).
4. B. Baschek, H. Holweger, and G. Traving, *Astronomische Abhandlung der Hamburger Sternwarte* **8**, 26–60 (1966).
5. B. Freytag, M. Steffen, H.-G. Ludwig, and S. Wedemeyer-Boehm, *Astrophysics Software Database* pp. 36–+ (2008).
6. H.-G. Ludwig, F. Allard, and P. H. Hauschildt, *A&A* **459**, 599–612 (2006).
7. P. H. Hauschildt, and E. Baron, *Journal of Computational and Applied Mathematics* **109**, 41–63 (1999).
8. M. Asplund, N. Grevesse, and A. J. Sauval, “The solar chemical composition,” in *ASP Conf. Ser. 336: Cosmic Abundances as Records of Stellar Evolution and Nucleosynthesis*, 2005, pp. 25–+.
9. J. W. Ferguson, D. R. Alexander, F. Allard, T. Barman, J. G. Bodnarik, P. H. Hauschildt, A. Heffner-Wong, and A. Tamanai, *APJ* **623**, 585–596 (2005).
10. B. Freytag, F. Allard, H. Ludwig, D. Homeier, and M. Steffen, *A&A* **in prep.** (2009).
11. P. Magain, *A&A* **163**, 135–139 (1986).
12. D. F. Gray, *APJ* **218**, 530–538 (1977).
13. D. F. Gray, *The Observation and Analysis of Stellar Photospheres*, The Observation and Analysis of Stellar Photospheres, by D.F. Gray. Cambridge: Cambridge University Press, 2008., 2008.
14. D. F. Gray, *APJ* **202**, 148–164 (1975).